Published online 26 November 2009

Nucleic Acids Research, 2010, Vol. 38, No. 3 ***e18***
doi:10.1093/nar/gkp1061

DNA structures from phosphate chemical shifts

Joséphine Abi-Ghanem[1], Brahim Heddi[2], Nicolas Foloppe[3,*] and Brigitte Hartmann[1,2,*]

[1]INTS, INSERM S-665, 6 rue Alexandre Cabanel, Paris 75015, [2]IBPC, CNRS UPR 9080, 13 rue Pierre et Marie Curie, Paris 75005, France and [3]51 Natal Road, Cambridge CB1 3NY, UK

Received June 30, 2009; Revised October 14, 2009; Accepted November 1, 2009

ABSTRACT

For B-DNA, the strong linear correlation observed by nuclear magnetic resonance (NMR) between the ^{31}P chemical shifts (δP) and three recurrent internucleotide distances demonstrates the tight coupling between phosphate motions and helicoidal parameters. It allows to translate δP into distance restraints directly exploitable in structural refinement. It even provides a new method for refining DNA oligomers with restraints exclusively inferred from δP. Combined with molecular dynamics in explicit solvent, these restraints lead to a structural and dynamical view of the DNA as detailed as that obtained with conventional and more extensive restraints. Tests with the Jun-Fos oligomer show that this δP-based strategy can provide a simple and straightforward method to capture DNA properties in solution, from routine NMR experiments on unlabeled samples.

INTRODUCTION

Nuclear magnetic resonance (NMR) is potentially the most powerful experimental method to investigate the structure and dynamics of macromolecules in solution. Traditionally, interproton distances extracted from nuclear Overhauser effect (NOE) measurements and scalar couplings are used as distance and torsion angle restraints in refinement. These conventional short-range restraints are now often supplemented by long-range information inferred from residual dipolar coupling (RDC) measurements that require oriented labeled molecules (1–5).

New methods using directly the chemical shifts have recently emerged, in particular, in the protein refinement context. These approaches were undertaken to model proteins that cannot be studied by conventional NMR but also to circumvent the long and tedious task to collect and analyze the NOE data. Indeed, the chemical shifts are particularly sensitive to the electronic environment and very accurately measured. However the difficulty is to interpret and translate these experimental observables into properties that can guide structural refinement protocols.

Thus, $^{13}C_\alpha$ chemical shifts, sensitive to protein secondary structure, have been proposed to improve protein models (6,7). Chemical shifts of C_α, C_β, H_α, H_β, H_N and C' are collectively used to define torsion angles (8,9). Reliable three-dimensional structures were obtained with NOE-derived distances supplemented by using $^{13}C_\alpha$ chemical shifts, measured and computed with a density functional approach, as a function of all backbone and side-chain torsional angles (10–13). However, the quantum calculations can be quite time consuming when applied to large molecules and simplifying the level of theory could degrade the accuracy of the resulting structures. Another approach, free of NOE restraints and minimizing the dependence on *ab initio* calculations, was recently proposed by Vendruscolo and co-authors (14,15). In their CHESHIRE protocol, the experimental chemical shifts are compared to an extensive structural database for determining analogs of short protein fragments, and predicting the most compatible dihedral restraints; the assembly of selected fragments from the database results in models then refined by molecular mechanics in conjunction with back-calculations of chemical shifts. Two approaches emanate from this strategy, either employing a Monte–Carlo algorithm for the reconstitution of the entire protein (9,16,17) or, for the CS-ROSSETTA method, an additional Monte–Carlo sampling coupled with an all-atom force field for the refinement (9,17). Chemical-shift-generated structures can be now generated via a web server (18). These strategies applied to high-resolution refinements are still limited to a few cases of relatively small proteins. Nevertheless, they appear very promising and open to further development.

With nucleic acids, the ^{13}C chemical shifts, earlier used to assess ε angles in the deoxyribonucleotide d(TpA) (19), enabled to determine sugar puckers and α/γ exocyclic

*To whom correspondence should be addressed. Email: brigitte.hartmann@univ-paris-diderot.fr
Correspondence may also be addressed to Nicolas Foloppe. Email: nf_research@hotmail.com
Present address:
Brahim Heddi, School of Physical & Mathematical Sciences, Nanyang Technological University, 21 Nanyang Link, SPMS PAP 05-08, Singapore 637371.

angles in ribo and deoxy-nucleotide units (20) and in RNA (21). In addition, they allowed to qualitatively detect perturbations in base-pairing and base-stacking (22) in RNA. ^{1}H chemical shifts associated to *ab initio* calculations were proposed for helping in the sequential assignment of resonances (23). ^{31}P chemical shifts (δP) and ^{3}J scalar dipolar couplings have been shown to improve the precision in refinement of large RNA molecules, by constraining dihedral angles (24). The δP anisotropy collected on labeled nucleic acids oriented in liquid crystals were also used to constrain the orientation of the phosphodiester groups relative to the molecular alignment tensor (25,26). However, it is not sure that constraining the B-DNA phosphodiester linkages in one orientation is pertinent, given that they are submitted to conformational transitions, as explained below. To our knowledge, no exploitation of chemical shifts for overall structure determination was reported for nucleic acids.

In this context, we propose a new and convenient strategy to refine nonlabeled B-DNA oligomers exclusively on the basis of their δP. In B-DNA in solution, some phosphate groups oscillate between two conformations, BI and BII (27–32). The BI↔BII transition corresponds to a crankshaft motion of the strongly correlated torsions ε and ζ, used to describe the two conformations, i.e. BI (ε = trans, ζ = g–, with $\varepsilon-\zeta=-90^{\circ}$) and BII (ε = g–, ζ = trans, with $\varepsilon-\zeta=+90^{\circ}$) (Figure 1). These two states, initially identified from crystallographic studies (33), were then detected in NMR by measurements of $^{3}J_{H3'\text{-}P}$ spin–spin coupling constants and/or δP (28,34–36). Because the ε/ζ crankshaft motions in solution are fast (35), the δP is a continuous function of the fraction of the BI and BII states. Theoretical studies (37,38), statistical analysis of X-ray structures (39,40) and recent NMR studies (41) showed separated energy minima for BI and BII, with transition barriers depending on the local dinucleotidic sequence.

The BI/BII ratio, inferred from δP, is primarily controlled at the dinucleotide level (29), confirming that the propensity to undergo the BI/BII transition is sequence dependent. Crucially, these phosphate states, the twist, the roll and the base displacement are intimately coupled (39,42–46). These relationships reflect the B-DNA intrinsic mechanics and can be captured in NMR by a marked linear correlation between δP and three internucleotide distances, $H2'_i$-$H6/8_{i+1}$ [ds(H2′)], $H2''_i$-$H6/8_{i+1}$ [ds(H2″)] and $H6/8_i$-$H6/8_{i+1}$ [ds(H6/8)] (29,47) (Figure 1). These correlations were used to translate the δP in terms of BI/BII ratios (29). Most importantly, they also allow to interpret δP in terms easily integrated in a structural refinement.

This approach was incipient in our recent refinement of the Jun-Fos DNA model system in solution, where δP-based restraints supplemented the set of conventional internucleotide restraints (48). This study first established that sugar conformations and orientations of bases compared to sugars (χ angles) are correctly treated in unrestrained molecular dynamics (MD). Therefore, they do not necessitate to be controlled by experimental data. The issue is to reliably manage the inter base-pair parameters, in particular the twist and the roll, and the BI↔BII motions, which cannot yet be predicted from unrestrained MD. However, due to the intrinsic B-DNA mechanics, these features can be together correctly driven by the experimental internucleotide distances (48). Overlaps in NMR spectra yet result in conventional restraints unevenly distributed along the sequence, with weakly restrained dinucleotide steps that are then predominantly under the influence of the force field. Therefore, distance restraints inferred from δP were added to traditional measured NOE distances, to compose a more extensive set of 'enhanced conventional' restraints. Combined with MD simulations, this 'enhanced conventional' approach increased the overall accuracy of the DNA structure. The representation of the backbone motions, poorly treated in unrestrained simulations, was especially improved (48).

These results inspired the new δP-based method presented here. This approach uses only the δP converted to distance restraints for the refinement of the Jun-Fos oligomer, well characterized in terms of structure and dynamics (29,47,48). We show that this new δP-based strategy is as reliable as the 'enhanced conventional' approach described above. This opens the prospect to probe conformational properties of nonlabeled B-DNA from routine NMR experiments, with substantial time savings regarding measurement time and spectral analysis compared to the classical approach using coupling constants and distances inferred from NOE measurements.

MATERIALS AND METHODS

DNA sequence

The Jun-Fos oligomer double-stranded DNA has the 14-bp sequence 5′-d(G_1 C_2 A_3 T_4 T_5 C_6 T_7 G_8 A_9 G_{10} T_{11} C_{12} A_{13} G_{14})-3′•5′-d(C_{15} T_{16} G_{17} A_{18} C_{19} T_{20} C_{21} A_{22} G_{23} A_{24} A_{25} T_{26} G_{27} C_{28})-3′. This system was previously characterized experimentally and structurally in details in solution (29,47,48). Thus, it was selected to test a new method for the structural refinement of DNA structures, which exploits NMR phosphate chemical shifts combined with MD simulations.

Phosphate chemical shifts interpreted in terms of distance restraints

In previous studies (29,47), the δP (Supplementary Table S1) were found linearly correlated to the three internucleotide distances $H2'_i$-$H6/8_{i+1}$ [ds(H2′)], $H2''_i$-$H6/8_{i+1}$ [ds(H2″)] and $H6/8_i$-$H6/8_{i+1}$ [ds(H6/8)], extracted from NOESY cross-peaks with particular care regarding to spin diffusion. This relation was also retrieved on X-ray structures (29), where the three internucleotide distances [ds(H2′)], [ds(H2″)] and [ds(H6/8)] correlated with $(\varepsilon-\zeta)$ which represents the BI and BII states. This ensures that no systematic NMR biases occur in our calibration of the relation between δP and the internucleotide distances of interest. These distances were extrapolated from δP (referenced to phosphoric acid) measured for the 22 phosphate groups of the

Jun-Fos oligomer (29), following the equations established from the correlations:

$$ds(H2') = \delta P/0.34 + 4.70$$

$$ds(H2'') = \delta P/0.47 + 3.94$$

$$ds(H6/8) = \delta P/0.29 + 5.86$$

NMR distance restraints

MD simulations were carried out under two sets of NMR internucleotide distance restraints termed *Res_total* and *Res_δP*. The 5′- and 3′-terminal dinucleotides were unrestrained. The 106 intranucleotide distances collected from NOESY cross-peaks were not restrained since they were spontaneously respected in all the MDs.

The *Res_total* set contained 100 internucleotide distances (Supplementary Table S2). These distances were used as restraints in a previous structural refinement work (48). Among them, 82 were directly derived from well-resolved NOESY cross-peaks (29): 48 $H2'_i$-$H6/8_{i+1}$, $H2''_i$-$H6/8_{i+1}$ and $H6/8_i$-$H6/8_{i+1}$, and 34 various distances ($H1'_i$-$H6/8'_{i+1}$, $H1'_i$-$H4'_{i+1}$, $H2_i$-$H1'_{i+1}$ and $H2'/2''_i$-$H5_{i+1}$). This pool was supplemented by 18 $H2'_i$-$H6/8_{i+1}$, $H2''_i$-$H6/8_{i+1}$ and $H6/8_i$-$H6/8_{i+1}$ distances, not directly measured but inferred from measured distances or from the corresponding δP. The experimental error was estimated to ±10% of the considered distance.

The second, new, set of restraints *Res_δP* consisted of 66 ds(H2′), ds(H2″) and ds(H6/8) internucleotide distances (three distances per dinucleotide step, defined earlier), all extrapolated from the corresponding δP.

To estimate the agreement between experimental NMR (*d_exp*) and theoretical MD (*d_theor*) distances, we calculated two descriptors of the fit between *d_exp* and *d_theor*. First, the overall similarity, comparing the profiles of *d_exp* and *d_theor* along the sequence, was assessed with the correlation coefficient *R* (calculated by linear regression) between *d_exp* and the averaged *d_theor* values, for different sets of relevant distances. Second, the average difference between *d_exp* and *d_theor* (Δ_*d*) was calculated. In addition, we consider that an individual distance violation occurs when the intervals *d_exp* ± 10% (±experimental error) and *d_theor* ± standard deviation (±SD) do not overlap.

MD simulations

Simulations were performed using the AMBER 8 program (49), with the Parm98 (50) force field. We previously found (48) that restrained simulations carried out with Parm98 led to a more realistic representation of the Jun-Fos oligomer than Parmbsc0 (51). The Jun-Fos oligomer in an initial AMBER standard B-DNA conformation was neutralized with 26 Na^+ ions and hydrated with 6770 TIP3P water molecules (52,53) in a truncated octahedron. Simulations were performed with periodic boundary conditions at constant temperature (300 K) and pressure (1 bar) using the Berendsen algorithm (54). The integration time-step was 2 fs and covalent bonds involving hydrogens were restrained using SHAKE (55). Long-range electrostatic interactions were treated using the particle mesh Ewald (PME) approach (56) with a 9-Å direct space cut-off. The Lennard-Jones interactions were cut off at a distance of 9 Å. The non-bonded pair-list was updated heuristically and the center-of-mass motion removed every 10 ps.

The water molecules and counterions were energy-minimized and equilibrated at 100 K around the fixed DNA for 100 ps in the NVT (at constant volume and temperature) ensemble; the entire system was then heated from 100 to 300 K in 10 ps by 5-K increments with harmonic positional restraints on the solute atoms (force-constant of 5.0 kcal/mol/Å^2). The simulation was continued in NPT (at constant pressure and temperature). The positional restraints were gradually removed over 250 ps and followed by 1 ns of unrestrained simulations for further equilibration.

The free MD of 1 ns yielded the starting point for the other, restrained, MD protocols. These restrained MDs were run in presence of NMR distance restraints described above, i.e. either *Res_total* (MD_ref) or *Res_δP* (MD_δP), for 15 ns (MD_ref) or 35 ns (MD_δP). These restraints were applied either instantaneously (MD_δP) or in time-averaged manner (MD_ref), via a mixed parabolic (for *d*_exp - 10%) and hyperbolic (for *d*_exp + 10%) potential around a central flat-bottomed well covering the experimental range of the distances, including experimental errors (*d*_exp ± 10%). The time-averaged restraints on property *R* were applied with the following equation:

$$R = (1/C)\{\int \exp[(t-t)/\tau] r(t')^{-i} dt'\}^{-1/i}$$

where t is the current time, $r(t')$ the internal coordinate at time t' and C a normalization factor. The damping constant τ was set to 10 ps and, following previous tests (48), the best results were for $i = 1$ used here. For the flat-bottomed harmonic potential, force constants of 5 (MD_ref and MD_δP) and 10 kcal/mol/Å^2 (MD_δP), were tested.

Convergence of the MDs with respect to the DNA structure was achieved. The root mean square deviation (RMSD) between snapshots and either the starting or the average structures were very stable after 1 ns of the restrained simulations. Statistics for the DNA descriptors (sugar and backbone conformations and inter-base pair parameters) give virtually identical results when they are extracted from different 10-ns blocks of the trajectories. Such analysis on MD_δP trajectory extended to 35 ns confirms that 15 ns are sufficient to reach convergence.

Crystallographic data

The crystal structures used in section 'Test 3: coupling between backbone states and helical parameters' and Figure 3 were comprised of 19 B-DNA oligomers with a resolution ≤2Å (PDB codes: 431D, 436D, 460D, 461D, 463D, 476D, 1D8G, 1DPN, 1EN3, 1EN8, 1EN9, 1ENE, 1ENN, 1EI4, 1FQ2, 5DNB, 1D23, 1D49 and 355D).

Structural descriptors

DNA structures and helicoidal parameters were analyzed with the Curves 6.1 algorithm (57,58), following the Cambridge convention (59). To avoid end effects, only the 12 central base-pairs (11 dinucleotides) were analyzed. The first nanosecond of each MD with NMR restraints was discarded.

RESULTS

Overview of the restraint sets and simulations

To present the different restraint sets pertaining to the present work, we summarize the experimental data obtained from our previous NMR study of the Jun-Fos oligomer (29). For the 11 central dinucleotides, the NMR spectra enabled to extract 106 intranucleotide distances, 82 internucleotide distances from NOE cross-peaks, 97 torsion angles from $^{3}J_{H1'-H2'}$, $^{3}J_{H3'-P}$, $^{3}J_{H5'-P}$, $^{3}J_{H5''-P}$ and $^{3}J_{H4'-P}$ scalar dipolar couplings, and all the BI/BII ratio from δP. 18 additional internucleotide distances were extrapolated from δP. The intranucleotide distances are sensitive to the χ torsions and to the sugar conformations, and the $^{3}J_{H1'-H2''}$, $^{3}J_{H5'-P}$, $^{3}J_{H5''-P}$ and $^{3}J_{H4'-P}$ scalar dipolar couplings, reflect the sugar conformations and the backbone angles β and γ. These intranucleotide distances do not vary significantly within a B-DNA devoid of disrupting features such as mismatches. Indeed, all of these observables were spontaneously respected in all the MDs carried out on the Jun-Fos oligomer (29,47,48), comprising unrestrained MDs (48). In contrast, neither the experimental internucleotide distances [mainly sensitive to the twist-and-roll parameters (60)], nor the experimental BI/BII ratios could be reproduced in unrestrained MD (48). Thus, they must be restrained during any refinement. $^{3}J_{H3'-P}$ values could be expressed in terms of ε angle restraints; however, it would not allow for the dynamics nature of the BI↔BII equilibrium. Still, due to the tight relationship between backbone motions and inter-base-pair parameters, the internucleotide distance restraints enable to indirectly control the BI/BII ratios, twist, roll and base displacement (48). In other words, the restraints crucial for B-oligomer refinement in general are the internucleotide distances.

Here, two set of restraints were used, *Res_total and Res_δP*. *Res_total* included a total of 100 internucleotide distance restraints (Supplementary Table S2), mainly of a conventional type, i.e. directly derived from NOESY cross-peaks ('NOE distances' hereafter). These experimental data correspond to 4.6 distances per dinucleotide step on average and represent ~67% of all theoretically possible internucleotide distances that could be routinely observed in the Jun-Fos oligomer. Restraints set *Res_δP* contained three types of internucleotide distances (Figure 1), ds(H2′), ds(H2″) and ds(H6/8), all inferred ('Materials and Methods' section) from the 22 δP previously measured (29); so the set *Res_δP* contains 66 (3×22) restraints. In *Res_total*, 48 of these distances were obtained from NOEs, and were compared to their counterpart in *Res_δP* inferred from δP. The distances derived from NOEs and δP differ by only 0.3 Å on average, present similar profiles along the sequence (Supplementary Figure S1), and are closely correlated (correlation coefficient of 0.92, slope of regression line of 0.9). Thus, *Res_δP* is congruent with *Res_total*.

The reference refinement (MD_ref) relied on a protocol that has already been shown to yield a detailed dynamical structure of the Jun-Fos oligomer in solution (48). MD_ref used *Res_total* time-averaged restraints because such restraints were slightly more realistic than when applied instantaneously (48). The δP-based protocol using *Res_δP* was tested with four variant simulations, presented in Supplementary Table S3. The best fit between experimental and simulated data was obtained with *Res_δP* distances applied instantaneously with a force constant of 10 kcal/mol/Å^2 for the parabolic potential (Supplementary Tables S4 and S5). This refinement, called MD_δP, is thus compared to MD_ref, the main objective being to assess if the new δP-based method (MD_δP) performs as well as the 'enhanced conventional' approach (MD_ref).

In each MD, the average RMSD between the snapshots and canonical B and A-DNA were <2.9 Å and >5.3 Å, respectively. These RMSD values show that the overall

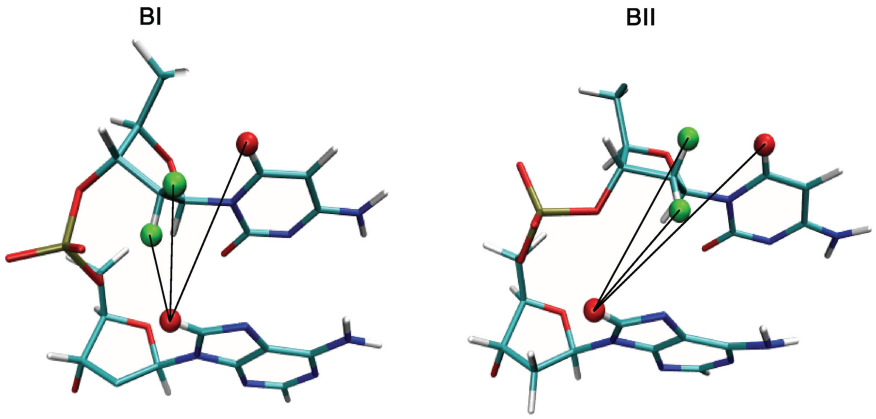

Figure 1. Illustration of the internucleotide distances ds(H2′), ds(H2″) and ds(H6/8) inferred from δP values. These distances depend on the phosphate linkage conformations, BI (left) or BII (right), as shown with a CpA dinucleotide. The black lines depict the internucleotide distances between H8 of the adenine (red) and H2′/H2″ (green) or H6 (red) of the cytosine.

Table 1. NMR experimental observables compared to their simulated counterpart

		MD_ref	MD_δP
ds(H2′) ds(H2″) ds(H6/8)	*R*	0.90	0.93
	Δ_*d*	0.3	0.3
'Other' distances	*R*	0.75	0.56
	Δ_*d*	0.35	0.5
BII percentage	*R*	0.70	0.93
	RMSD	21	15

Experimental NMR observables for the Jun-Fos oligomer include internucleotide distances measured from NOE spectra and the percentage of BII conformation for every phosphate. These observables are compared to their simulated counterpart, whether obtained with a conventional refinement protocol (MD_ref) or with the δP-based method (MD_δP). The NOE distances are divided into a group of distances restrained in the two MDs [ds(H2′), ds(H2″) and ds(H6/8)] and the distances ('Other' distances) restrained in MD_ref but not in MD_δP. The correlation coefficients (*R*) and the average differences (Δ_*d* in Å) between NMR and simulated distances are given for each distance category, across MDs. The RMSD between the experimental and simulated BII percentages was calculated as: $RMSD = [\Sigma(\%BII_{theo} - \%BII_{exp})^2 / N]^{1/2}$, with $N = 22$, number of phosphate. The best and worst values of the RMSD would be 0 and 100, respectively.

simulated structures were stable in the B form, consistent with the NMR data.

Test 1: backbone conformation and directly coupled distances

This section compares the distances modeled in simulations MD_δP to their NOE counterparts, used in MD_ref. MD_ref is thus also used for comparison to MD_δP. It is then natural to extend this comparison to the related BI/BII populations, between MD_δP, MD_ref and their experimental references.

The 48 NOE distances ds(H2′), ds(H2″) and ds(H6/8) are well reproduced in MD_δP (Table 1). This satisfying correspondence is illustrated in Figure 2 that compares the experimental and simulated ds(H2′), ds(H2″) and ds(H6/8) for MD_ref and MD_δP. Introducing the distances ds(H2′), ds(H2″) and ds(H6/8) as restraints acts on the backbone behavior, i.e. the BI↔BII equilibrium (Figure 1) (48). The δP, collected for all the Jun-Fos oligomer phosphate groups, reflect the diversity of local flexibilities along this B-DNA sequence, from 0 (δP of –0.70) to 85% (δP of 0.00) of BII conformers (Supplementary Table S1 and Figure S2). These NMR

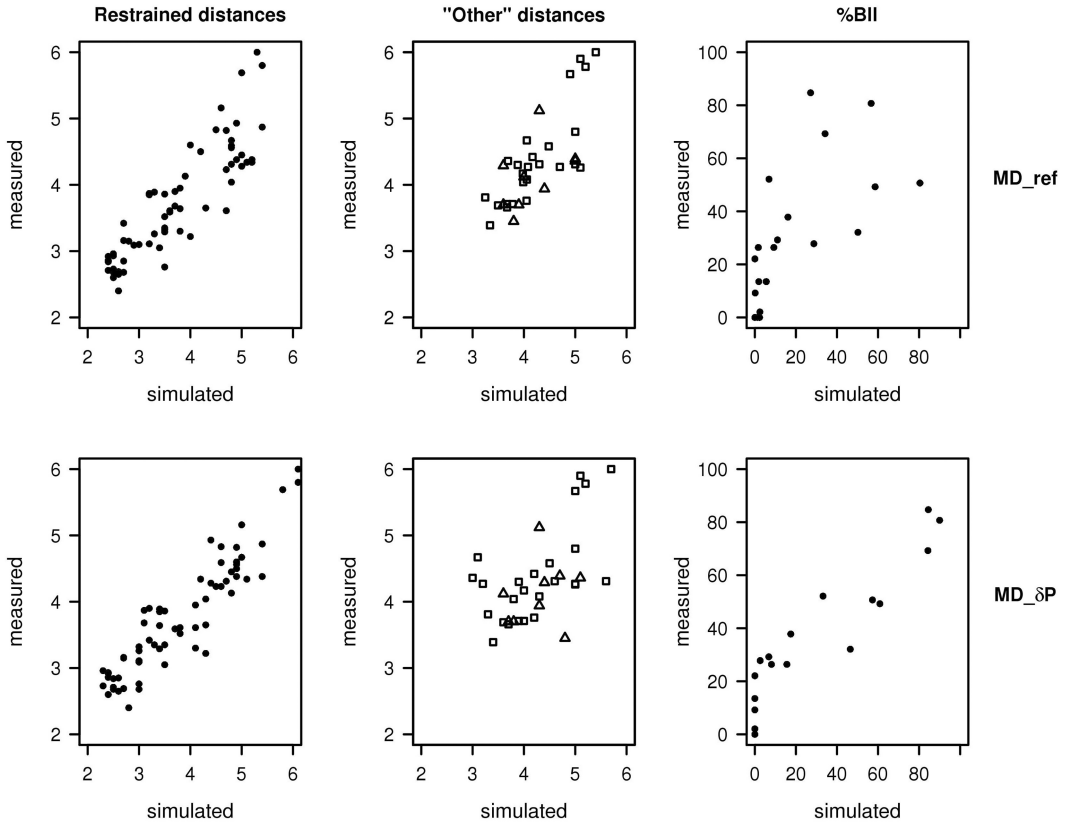

Figure 2. Plots of simulated versus measured distances and BII populations. Measured internucleotide distances (Å) and BII populations (in percent) in the Jun-Fos oligomer were extracted from NOESY cross-peaks and from δP, respectively. These observables are compared to their simulated counterpart, whether obtained with a conventional refinement protocol (MD_ref) or with the new δP-based method (MD_δP). The NOE distances are divided into a group restrained in all MDs [ds(H2′), ds(H2″) and ds(H6/8)] (leftmost panels) and the 'Other' distances restrained in MD_ref but not in MD_δP (middle panels). In 'Other' distances, $H2_i$-$H1'_{i+1}$ and $H2'/2''_i$-$H5_{i+1}$ correspond to symbols Δ, and $H1'_i$-$H6/8_{i+1}$ and $H1'_i$-$H4'_{i+1}$ to symbols □.

data show that the steps conductive to BII are TpG (26–52% of BII), their complementary CpA (69–85% BII) and GpA (32–52% BII), all located in the TGA stretches of the Jun-Fos oligomer (29,47). The other phosphate groups of the oligomer remain essentially trapped in BI. Besides, unusual α/γ conformations are observed neither in NMR (29) nor in the present simulations, suggesting that the corresponding force-field artifact (29,51,61,62) may be circumvented under restraints. The experimental BI/BII percentages are especially well retrieved in MD_δP (Table 1, Figure 2 and Supplementary Figure S2). This proper representation of the backbone motions is clearly the result of the well-respected restraints *Res_δP* having a desirable impact, as unrestrained MDs performed poorly in the same comparison with experiment (48).

Test 2: distances not explicitly restrained in MD_δP

We now compare to experiment (when available) the distances unrestrained in the MD_δP refinement, which is crucial to validate the δP-based approach. Indeed, it is of great interest to see if *Res_ δP* is enough to maintain all aspects of the DNA structure within the experimental regime.

The global characteristics of the B-DNA form (χ angle and predominance of *south* sugar conformations) are well respected in unrestrained MD (48). Moreover, the simulated intranucleotide distances, sensitive to these parameters, are highly correlated to the corresponding 106 distances extracted from NOESY cross-peaks (correlation coefficients $\geq$ 0.9) in MD_ref and MD_δP. Therefore, the intranucleotide distances are properly treated by the force field alone in absence of restraints.

We now turn to the 34 internucleotide NOE distances restrained in MD_ref but not in MD_δP. Most of them were not spontaneously respected in the unrestrained MD (48). In Table 1 and Figure 2 these distances are in the category 'Other' distances.

In MD_δP, these unrestrained distances are reasonably close to experiment (Table 2, Figure 2). Some of these distances are characteristic of adenines ($H2_i$-$H1'_{i+1}$) and cytosines ($H2'/2''_i$-$H5_{i+1}$). The analysis of very-high-resolution X-ray DNA structures reveals that these distances are in fact coupled with ds(H2′), ds(H2″) and ds(H6/8) (correlation coefficients of 0.8–0.9) and thus respond indirectly to the restraints in MD_δP. The distances $H1'_i$-$H6/8_{i+1}$ and $H1'_i$-$H4'_{i+1}$ are sensitive to the conformations of two successive sugars (60). In all the simulations the unrestrained sugars were mainly in *south*, with *south* percentages higher for purines (>90%) than pyrimidines (>70%), in agreement with NMR (25,29,63,64). This concordance is sufficient to avoid severe violations on $H1'_i$-$H6/8_{i+1}$ and $H1'_i$-$H4'_{i+1}$ in MD_δP. However, the correlation between experimental and simulated distances is better in MD_ref than in MD_δP (Table 1). Yet, this does not degrade the representation of the helicoidal parameters in MD_δP, as examined in the next section.

Table 2. Conformational families for the Jun-Fos oligomer

Conformational family	BI/***BII*** configurations	NMR	MD_ref	MD_δP
1	TpG***p***A ApCpT	≤15	33	2
2	TpGpA ApCpT		28	3
3	TpGpA A***p***CpT	≤15	16	16
4	TpG***p***A A***p***CpT	33–48	14	56
5	T***p***GpA A***p***CpT	37	5	20

The five conformational families of the Jun-Fos oligomer and their populations (percentage) were previously deduced from NMR (48). The phosphate configurations (***BII*** in bold italic) observed on the TpGpA regions are a distinctive feature of each family (48). For MD_ref and MD_δP, the population of each family is compared with the experimental populations.

Test 3: coupling between backbone states and helical parameters

A common method to check the reliability of simulated DNA structures is to compare their average inter-base helical parameters values with those extracted from X-ray structures. A more detailed approach is to analyze whether the simulations satisfactorily reproduced the well-documented couplings between the helical parameters, twist, roll and base displacement (X-disp), and the backbone BI/BII states (29,39,42,45,46,48,65).

The average values of the roll and twist were extracted for the three possible combinations BI•BI, BI•BII and BII•BII encountered on complementary dinucleotides, from the MD snapshots and from a set of high-resolution X-ray structures of free B-DNA. We focus on CpA•TpG steps because they populate the three different facing phosphate combinations. Overall, the MD models reflect the general trend observed in X-ray structures: in both MD_ref and MD_δP, the greater the BII character of facing phosphates in a complementary dinucleotide, the higher the twist and the more negative the roll (Figure 3).

In addition, several proximal phosphates in BII are typically accompanied by a displacement of bases towards the major groove (more positive X-disp) that propagates to neighboring bases to maintain sufficient stacking (37,46). Therefore, the global X-disp values are sensitive to the density of BII steps, i.e. the fraction of phosphates observed simultaneously in BII. In high-resolution X-ray structures the global X-disp of a purely BI oligomer is −1.4 Å, but it is null or positive with more than 25% of BII steps. These trends are equally well represented in MD_ref and MD_δP, with X-disp of −1.7 Å for a pure BI configuration and X-disp of −0.6 with 32% of BII phosphates (7 BII and 15 BI), for both MD_ref and MD_δP.

In sum, the MD_δP protocol represents correctly the intrinsic mechanical couplings of B-DNA, providing a sound basis to address the conformational dynamics of the Jun-Fos oligomer.

Test 4: the dynamical structure of the Jun-Fos oligomer

Arguably, the most stringent test of the δP-based method is whether it yields the overall correct structural dynamics of DNA in solution. Having a precise representation of

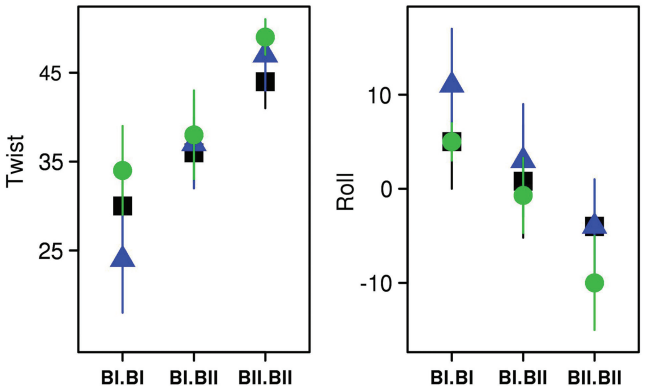

Figure 3. Impact of the conformation of facing phosphate groups on key helical descriptors. The average values of twist (°) and roll (°) of the Jun-Fos oligomer TpG•CpA steps are plotted as a function of the three possible conformational combinations of facing phosphates, BI•BI, BI•BII and BII•BII. The data were extracted from a set of high-resolution X-ray structures (green), from MD_ref (blue) and MD_δP (black).

backbone behavior makes it possible to identify distinct conformational families. Indeed, some simple guiding rules have emerged about the DNA backbone dynamics, from theoretical (42,66), X-ray (39,42) and NMR (48,63) studies. Thus, two phosphates adjacent on a strand do not stay in BII simultaneously. Instead, phosphates facing each other on opposing strands tend to populate BII simultaneously. In the Jun-Fos oligomer, these rules applied to the central BII-rich stretch TpGpA•TpCpA enabled to identify five families (48). These families and their individual populations assessed from the NMR data are reported in Table 2.

MD_ref could retrieve these five families but not their experimental populations (48) (Table 2). MD_δP also identified the five main conformational families (Table 2). In addition, their populations compared well to the NMR estimates (Table 2), consistent with the very good agreement between measured and simulated BII percentages (Figure 2, Table 1). However, this apparently better representation of the populations by MD_δP may be fortuitous, and more tests with other systems will be needed to address this question more robustly.

Sorting the snapshots into families on the basis of their BI/BII combinations enables to calculate average structures for each family without generating 'virtual conformers' with distorted torsions. These average structures can thus be used to characterize each structural family, that, taken together, illustrate the conformational space explored by the oligomer.

The five families generated by MD_δP are very close to those from MD_ref. The mean RMSD between the average family structures from MD_δP and MD_ref is 0.7 ± 0.3 Å. Indeed, the previously described structural characteristics of the Jun-Fos oligomer in solution (48) are all retrieved by MD_δP. Thus, the twist-and-roll profiles along the Jun-Fos sequence for each conformational family show that the BI ↔ BII exchanges impart a highly variable structure to the T_5-A_9 region, in both MD_δP and MD_ref (Figure 4). Family 5 is especially distinctive, with undulating roll and twist profiles. In addition, the five structural categories present significant differences in groove dimensions, via the BI/BII effect on X-disp (see above and Supplementary Figure S3). For example, in family 5 the two BII phosphates in TGA impart to the DNA a deep and rather narrow minor groove and a shallow and wide major groove, compared to family 2 (no BII in TGA).

That MD_δP captures the helicoidal features in each family as well as MD_ref is an important point, as there is evidence that the structural characteristics of family 5 parallel those of the DNA bound to the Jun-Fos transcription factor (48).

DISCUSSION

The main objective of this work is to propose a new method for refining DNA structure in solution with NMR δP as the sole experimental input, combined with MD simulation techniques. The Jun-Fos oligomer is an appropriate system to test the new method, as much information has accumulated about its structure and dynamics in solution (29,47,48). The Jun-Fos structure in solution cannot be obtained directly from unrestrained MD simulations with current force-field limitations (48), and appropriate experimental input is required.

At its core, this new δP-based method simply relies on the strong linear correlations in B-DNA between δP and the internucleotide distances ds(H2′), ds(H2″) and ds(H6/8) (29,47). These correlations allow to translate any δP in terms of three distance restraints, following simple equations previously established (29) (reiterated in 'Materials and Methods' section).

Having constituted a set of restraints exclusively inferred from δP, we showed that all the distances extracted from the corresponding MD_δP refinement reproduced well the experimental data. Cross-correlations between restrained and unrestrained distances, together with the adequate treatment of the generic B-DNA features by the force field, largely explain why the δP-based method yields a good agreement between measured and simulated DNA distances. In addition, MD_δP correctly represents the BI/BII backbone states, accounts for the DNA intrinsic mechanics, i.e. the relationships between BI/BII ratio and the helicoidal parameters (twist, roll, base displacement) and allows the characterization of the Jun-Fos conformational families in solution. In sum, compared to the reference conventional refinement, the δP-based refinement can generate credible representations of DNA structure and dynamics in solution.

The δP-based method does not require labeled DNA or NOE measurements. Furthermore, it circumvents imprecisions in distances restraints inferred from NOEs, which can be introduced via spin diffusion and require very careful treatment of data. One limitation concerns the problem of repeated or large (>20 bp) sequences generating considerable overlaps and/or anisotropic overall motions that prevent the assignment of all the ^{31}P and ^{1}H resonances. This restriction is not particular

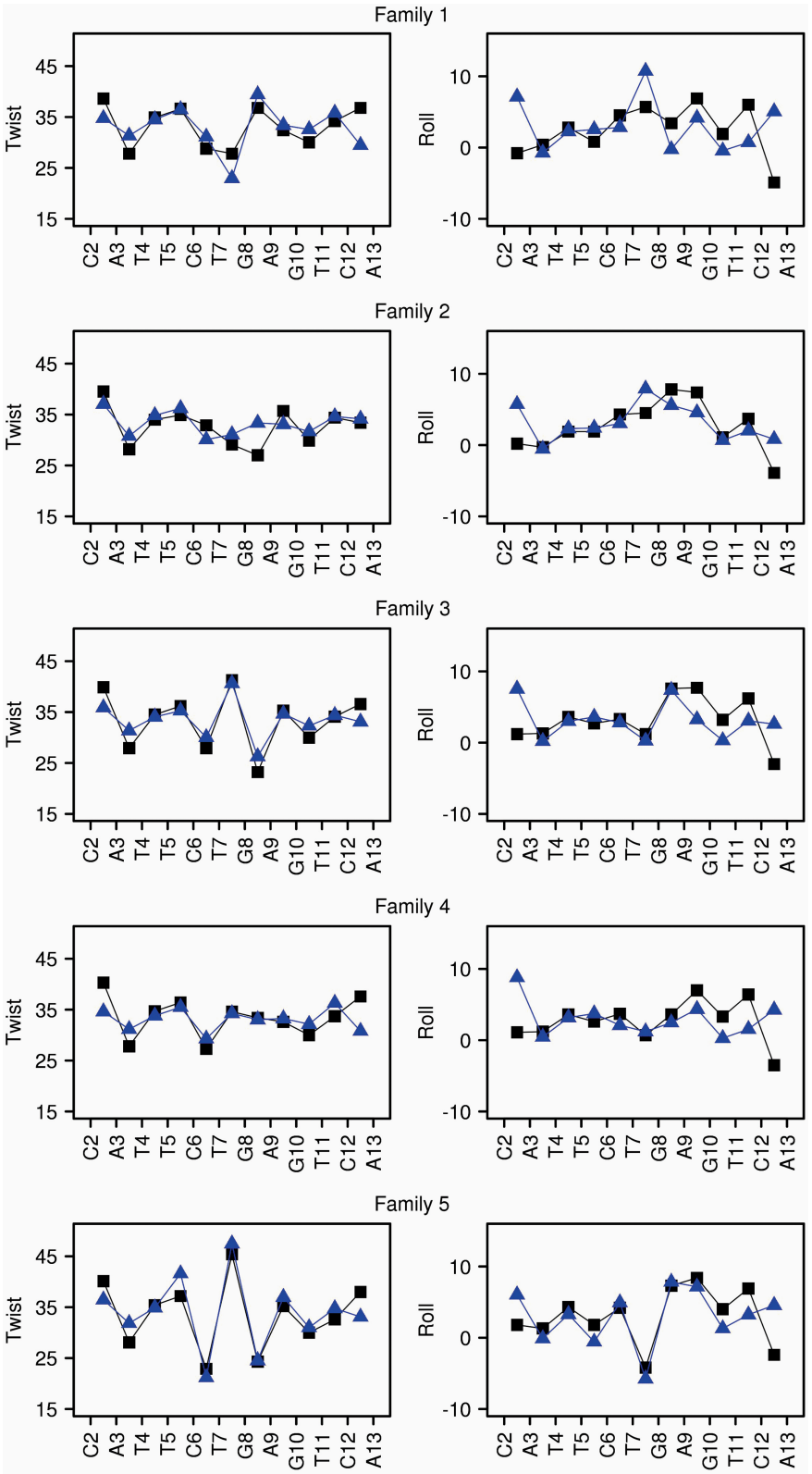

Figure 4. Structure and dynamics of the Jun-Fos oligomer in terms of conformational families. Conformational families 1–5 (from top to bottom, defined in Table 2) are characterized in terms of twist and roll profiles along the oligomer sequence. Twist (°) and roll (°) average values were extracted from MD_ref (blue) and MD_δP (black). The standard deviations of twists and rolls are 5°. The DNA sequence is represented by its first strand in the *X*-axis, but both strands were included in the calculations.

to the δP-based method, and these DNAs require specific labeling and RDC measurements in oriented medium to be reliably refined (3).

To our knowledge, the δP-based method demonstrates for the first time how to exploit chemical shifts as the main experimental basis to refine B-DNA structures. This is an alternative to the classical method based on numerous NOE measurements. The chemical shifts are generally available at the early stage of an NMR structure determination, before the collection and analysis of NOE cross-peaks. It would be desirable to further probe if the data extracted from well-resolved spectra on nonlabeled oligomers can describe the subtle features of B-oligomers by comparing our results to additional RDC data using labeled samples. In particular, the DNA curvature, very difficult to evaluate even with RDC, should be carefully checked. Nevertheless, at the present stage, the δP-based method is simpler than a conventional approach, and offers substantial time savings in terms of experimental measurements and data treatments. This could significantly increase the throughput of the structural characterization of DNA sequences for systematic structural biology analyses, for instance the study of protein target sites and their mutants that are typically B-DNA of 10–15 bp. This is indeed a pressing need, considering the vast amount of sequences now available for biological interpretation.

SUPPLEMENTARY DATA

Supplementary Data are available at NAR Online.

FUNDING

Funding for open access charge: Institut National de la Transfusion Sanguine (INTS), France.

Conflict of interest statement. None declared.

REFERENCES

1. Bax,A. and Grishaev,A. (2005) Weak alignment NMR: a hawk-eyed view of biomolecular structure. *Curr. Opin. Struct. Biol.*, **15**, 563–570.
2. Getz,M., Sun,X., Casiano-Negroni,A., Zhang,Q. and Al-Hashimi,H.M. (2007) NMR studies of RNA dynamics and structural plasticity using NMR residual dipolar couplings. *Biopolymers*, **86**, 384–402.
3. Lipsitz,R.S. and Tjandra,N. (2004) Residual dipolar couplings in NMR structure analysis. *Annu. Rev. Biophys. Biomol. Struct.*, **33**, 387–413.
4. MacDonald,D. and Lu,P. (2002) Residual dipolar couplings in nucleic acid structure determination. *Curr. Opin. Struct. Biol.*, **12**, 337–343.
5. Tjandra,N. and Bax,A. (1997) Direct measurement of distances and angles in biomolecules by NMR in a dilute liquid crystalline medium. *Science*, **278**, 1111–1114.
6. Ikura,M., Spera,S., Barbato,G., Kay,L.E., Krinks,M. and Bax,A. (1991) Secondary structure and side-chain 1H and 13C resonance assignments of calmodulin in solution by heteronuclear multidimensional NMR spectroscopy. *Biochemistry*, **30**, 9216–9228.
7. Wishart,D.S., Sykes,B.D. and Richards,F.M. (1991) Relationship between nuclear magnetic resonance chemical shift and protein secondary structure. *J. Mol. Biol.*, **222**, 311–333.
8. Cornilescu,G., Delaglio,F. and Bax,A. (1999) Protein backbone angle restraints from searching a database for chemical shift and sequence homology. *J. Biomol. NMR*, **13**, 289–302.
9. Shen,Y., Vernon,R., Baker,D. and Bax,A. (2009) De novo protein structure generation from incomplete chemical shift assignments. *J. Biomol. NMR*, **43**, 63–78.
10. Iwadate,M., Asakura,T. and Williamson,M.P. (1999) C alpha and C beta carbon-13 chemical shifts in proteins from an empirical database. *J. Biomol. NMR*, **13**, 199–211.
11. Vila,J.A., Aramini,J.M., Rossi,P., Kuzin,A., Su,M., Seetharaman,J., Xiao,R., Tong,L., Montelione,G.T. and Scheraga,H.A. (2008) Quantum chemical 13C(alpha) chemical shift calculations for protein NMR structure determination, refinement, and validation. *Proc. Natl Acad. Sci. USA*, **105**, 14389–14394.
12. Vila,J.A., Ripoll,D.R. and Scheraga,H.A. (2007) Use of 13Calpha chemical shifts in protein structure determination. *J. Phys. Chem. B*, **111**, 6577–6585.
13. Wilton,D.J., Tunnicliffe,R.B., Kamatari,Y.O., Akasaka,K. and Williamson,M.P. (2008) Pressure-induced changes in the solution structure of the GB1 domain of protein G. *Proteins*, **71**, 1432–1440.
14. Cavalli,A., Salvatella,X., Dobson,C.M. and Vendruscolo,M. (2007) Protein structure determination from NMR chemical shifts. *Proc. Natl Acad. Sci. USA*, **104**, 9615–9620.
15. Montalvao,R.W., Cavalli,A., Salvatella,X., Blundell,T.L. and Vendruscolo,M. (2008) Structure determination of protein–protein complexes using NMR chemical shifts: case of an endonuclease colicin-immunity protein complex. *J. Am. Chem. Soc.*, **130**, 15990–15996.
16. Gong,H., Shen,Y. and Rose,G.D. (2007) Building native protein conformation from NMR backbone chemical shifts using Monte Carlo fragment assembly. *Protein Sci.*, **16**, 1515–1521.
17. Shen,Y., Lange,O., Delaglio,F., Rossi,P., Aramini,J.M., Liu,G., Eletsky,A., Wu,Y., Singarapu,K.K., Lemak,A. *et al.* (2008) Consistent blind protein structure generation from NMR chemical shift data. *Proc. Natl Acad. Sci. USA*, **105**, 4685–4690.
18. Wishart,D.S., Arndt,D., Berjanskii,M., Tang,P., Zhou,J. and Lin,G. (2008) CS23D: a web server for rapid protein structure generation using NMR chemical shifts and sequence data. *Nucleic Acids Res.*, **36**, W496–W502.
19. Lankhorst,P.P., Haasnoot,C.A., Erkelens,C. and Altona,C. (1984) Carbon-13 NMR in conformational analysis of nucleic acid fragments. 3. The magnitude of torsional angle epsilon in d(TpA) from CCOP and HCOP NMR coupling constants. *Nucleic Acids Res.*, **12**, 5419–5428.
20. Xu,X.-P., Chiu,W.-L.A.K. and Au-Yeung,S.C.F. (1998) Chemical shift and structure relationship in nucleic acids: correlation of backbone torsion angles γ and α with ^{13}C chemical shifts. *J. Am. Chem. Soc.*, **120**, 4230–4231.
21. Ohlenschlager,O., Haumann,S., Ramachandran,R. and Gorlach,M. (2008) Conformational signatures of 13C chemical shifts in RNA ribose. *J. Biomol. NMR*, **42**, 139–142.
22. Fares,C., Amata,I. and Carlomagno,T. (2007) 13C-detection in RNA bases: revealing structure-chemical shift relationships. *J. Am. Chem. Soc.*, **129**, 15814–15823.
23. Wijmenga,S.S., Kruithof,M. and Wilbers,C.W. (1997) Analysis of ^{1}H chemical shifts in DNA: assessment of the reliability of ^{1}H chemical shift calculations for use in structure refinement. *J. Biomol. NMR*, **10**, 337–350.
24. Allain,F.H. and Varani,G. (1997) How accurately and precisely can RNA structure be determined by NMR? *J. Mol. Biol.*, **267**, 338–351.
25. Wu,Z., Delaglio,F., Tjandra,N., Zhurkin,V.B. and Bax,A. (2003) Overall structure and sugar dynamics of a DNA dodecamer from homo- and heteronuclear dipolar couplings and 31P chemical shift anisotropy. *J. Biomol. NMR*, **26**, 297–315.
26. Wu,Z., Tjandra,N. and Bax,A. (2001) ^{31}P chemical shift anisotropy as an aid in determining nucleic acid structure in liquid crystals. *J. Am. Chem. Soc.*, **123**, 3617–3618.
27. Chou,S.H., Cheng,J.W. and Reid,B.R. (1992) Solution structure of [d(ATGAGCGAATA)]2. Adjacent G:A mismatches stabilized by cross-strand base-stacking and BII phosphate groups. *J. Mol. Biol.*, **228**, 138–155.
28. Gorenstein,D.G. (1984) *Phosphorus-31 NMR: Principles and Applications*. Academic Press, New York.

29. Heddi,B., Foloppe,N., Bouchemal,N., Hantz,E. and Hartmann,B. (2006) Quantification of DNA BI/BII backbone states in solution. Implications for DNA overall structure and recognition. *J. Am. Chem. Soc.*, **128**, 9170–9177.
30. Lefebvre,A., Mauffret,O., Lescot,E., Hartmann,B. and Fermandjian,S. (1996) Solution structure of the CpG containing d(CTTCGAAG)2 oligonucleotide: NMR data and energy calculations are compatible with a BI/BII equilibrium at CpG. *Biochemistry*, **35**, 12560–12569.
31. Tisne,C., Hantz,E., Hartmann,B. and Delepierre,M. (1998) Solution structure of a non-palindromic 16 base-pair DNA related to the HIV-1 kappa B site: evidence for BI-BII equilibrium inducing a global dynamic curvature of the duplex. *J. Mol. Biol.*, **279**, 127–142.
32. Tisne,C., Hartmann,B. and Delepierre,M. (1999) NF-kappa B binding mechanism: a nuclear magnetic resonance and modeling study of a GGG –> CTC mutation. *Biochemistry*, **38**, 3883–3894.
33. Fratini,A.V., Kopka,M.L., Drew,H.R. and Dickerson,R.E. (1982) Reversible bending and helix geometry in a B-DNA dodecamer: CGCGAATTBrCGCG. *J. Biol. Chem.*, **257**, 14686–14707.
34. Gorenstein,D.G. (1992) 31P NMR of DNA. *Methods Enzymol.*, **211**, 254–286.
35. Gorenstein,D.G. (1994) Conformation and dynamics of DNA and protein–DNA complexes by 31P NMR. *Chem. Rev.*, **94**, 1315–1338.
36. Lankhorst,P.P., Haasnoot,C.A., Erkelens,C. and Altona,C. (1984) Carbon-13 NMR in conformational analysis of nucleic acid fragments. 2. A reparametrization of the Karplus equation for vicinal NMR coupling constants in CCOP and HCOP fragments. *J. Biomol. Struct. Dyn.*, **1**, 1387–1405.
37. Bertrand,H., Ha-Duong,T., Fermandjian,S. and Hartmann,B. (1998) Flexibility of the B-DNA backbone: effects of local and neighbouring sequences on pyrimidine-purine steps. *Nucleic Acids Res.*, **26**, 1261–1267.
38. Foloppe,N. and MacKerell,A. (1999) Contribution of the phosphodiester backbone and glycosyl linkage intrinsic torsional energetics to DNA structure and dynamics. *J. Phys. Chem. B*, **103**, 10955–10964.
39. Djuranovic,D. and Hartmann,B. (2003) Conformational characteristics and correlations in crystal structures of nucleic acid oligonucleotides: evidence for sub-states. *J. Biomol. Struct. Dyn.*, **20**, 771–788.
40. Elsawy,K.M., Hodgson,M.K. and Caves,L.S. (2005) The physical determinants of the DNA conformational landscape: an analysis of the potential energy surface of single-strand dinucleotides in the conformational space of duplex DNA. *Nucleic Acids Res.*, **33**, 5749–5762.
41. Tian,Y., Kayatta,M., Shultis,K., Gonzalez,A., Mueller,L.J. and Hatcher,M.E. (2009) (31)P NMR investigation of backbone dynamics in DNA binding sites (dagger). *J. Phys. Chem. B*, **113**, 2596–2603.
42. Djuranovic,D. and Hartmann,B. (2004) DNA fine structure and dynamics in crystals and in solution: the impact of BI/BII backbone conformations. *Biopolymers*, **73**, 356–368.
43. Hartmann,B., Piazzola,D. and Lavery,R. (1993) BI-BII transitions in B-DNA. *Nucleic Acids Res.*, **21**, 561–568.
44. Srinivasan,A.R. and Olson,W.K. (1987) Nucleic acid model building: the multiple backbone solutions associated with a given base morphology. *J. Biomol. Struct. Dyn.*, **4**, 895–938.
45. van Dam,L. and Levitt,M.H. (2000) BII nucleotides in the B and C forms of natural-sequence polymeric DNA: a new model for the C form of DNA. *J. Mol. Biol.*, **304**, 541–561.
46. Winger,R.H., Liedl,K.R., Pichler,A., Hallbrucker,A. and Mayer,E. (1999) Helix morphology changes in B-DNA induced by spontaneous B(I)<==>B(II) substrate interconversion. *J. Biomol. Struct. Dyn.*, **17**, 223–235.
47. Heddi,B., Foloppe,N., Hantz,E. and Hartmann,B. (2007) The DNA structure responds differently to physiological concentrations of K(+) or Na(+). *J. Mol. Biol.*, **368**, 1403–1411.
48. Heddi,B., Foloppe,N., Oguey,C. and Hartmann,B. (2008) Importance of accurate DNA structures in solution: the Jun-Fos model. *J. Mol. Biol.*, **382**, 956–970.
49. Case,D.A., Cheatham,T.E. III, Darden,T., Gohlke,H., Luo,R., Merz,K.M. Jr, Onufriev,A., Simmerling,C., Wang,B. and Woods,R.J. (2005) The Amber biomolecular simulation programs. *J. Comput. Chem.*, **26**, 1668–1688.
50. Cheatham,T.E. III, Cieplak,P. and Kollman,P.A. (1999) A modified version of the Cornell *et al.* force field with improved sugar pucker phases and helical repeat. *J. Biomol. Struct. Dyn.*, **16**, 845–862.
51. Perez,A., Marchan,I., Svozil,D., Sponer,J., Cheatham,T.E. III, Laughton,C.A. and Orozco,M. (2007) Refinement of the AMBER force field for nucleic acids: improving the description of alpha/gamma conformers. *Biophys. J.*, **92**, 3817–3829.
52. Jorgensen,W.L., Chandrasekhar,J. and Madura,J.D. (1983) Comparison of simple potential functions for simulating liquid water. *J. Chem. Phys.*, **79**, 926–935.
53. Mahoney,W. and Jorgensen,L.W. (2000) A five-site model for liquid water and the reproduction of the density anomaly by rigid, nonpolarizable potential functions. *J. Chem. Phys.*, **112**, 8910–8922.
54. Berendsen,H.J.C., Postma,J.P.M., van Gunsteren,W.F., DiNola,A. and Haak,J.R. (1984) Molecular dynamics with coupling to an external bath. *J. Chem. Phys.*, **81**, 3684–3690.
55. van Gunsteren,W.F. and Berendsen,H.J.C. (1977) Algorithms for macromolecular dynamics and constraint dynamics. *Mol. Phys.*, **34**, 1311–1327.
56. Darden,T., York,D. and Pedersen,L. (1993) Particle mesh Ewald: an Nlog(N) method for Ewald sums in large systems. *J. Chem. Phys.*, **98**, 10089–10092.
57. Lavery,R. and Sklenar,H. (1988) The definition of generalized helicoidal parameters and of axis curvature for irregular nucleic acids. *J. Biomol. Struct. Dyn.*, **6**, 63–91.
58. Stofer,E. and Lavery,R. (1994) Measuring the geometry of DNA grooves. *Biopolymers*, **34**, 337–346.
59. Dickerson,R.E., Bansal,M., Calladine,C.R., Diekmann,S., Hunter,W.N., Kennard,O., von Kitzing,E., Lavery,R., Nelson,H.C.M., Olson,W.K. *et al.* (1989) Definition and nomenclature of nucleic acid structure parameters. *EMBO J.*, **8**, 1–4.
60. Lefebvre,A., Fermandjian,S. and Hartmann,B. (1997) Sensitivity of NMR internucleotide distances to B-DNA conformation: underlying mechanics. *Nucleic Acids Res.*, **25**, 3855–3862.
61. Beveridge,D.L., Barreiro,G., Byun,K.S., Case,D.A., Cheatham,T.E. III, Dixit,S.B., Giudice,E., Lankas,F., Lavery,R., Maddocks,J.H. *et al.* (2004) Molecular dynamics simulations of the 136 unique tetranucleotide sequences of DNA oligonucleotides. I. Research design and results on d(CpG) steps. *Biophys. J.*, **87**, 3799–3813.
62. Varnai,P., Djuranovic,D., Lavery,R. and Hartmann,B. (2002) Alpha/gamma transitions in the B-DNA backbone. *Nucleic Acids Res.*, **30**, 5398–5406.
63. Isaacs,R.J. and Spielmann,H.P. (2001) NMR evidence for mechanical coupling of phosphate B(I)-B(II) transitions with deoxyribose conformational exchange in DNA. *J. Mol. Biol.*, **311**, 149–160.
64. Schmitz,U., Ulyanov,N.B., Kumar,A. and James,T.L. (1993) Molecular dynamics with weighted time-averaged restraints for a DNA octamer. Dynamic interpretation of nuclear magnetic resonance data. *J. Mol. Biol.*, **234**, 373–389.
65. Tisne,C., Delepierre,M. and Hartmann,B. (1999) How NF-kappaB can be attracted by its cognate DNA. *J. Mol. Biol.*, **293**, 139–150.
66. Djuranovic,D. and Hartmann,B. (2005) Molecular dynamics studies on free and bound targets of the bovine papillomavirus type I e2 protein: the protein binding effect on DNA and the recognition mechanism. *Biophys. J.*, **89**, 2542–2551.